Application of wave-induced vertical mixing to the K profile parameterization scheme

Yonggang Wang,[1] Fangli Qiao,[1] Guohong Fang,[1] and Zexun Wei[1]

Received 28 September 2009; revised 20 April 2010; accepted 28 April 2010; published 16 September 2010.

[1] Surface-wave-induced vertical mixing is incorporated to modify the K profile parameterization (KPP) scheme. The effects of this modified KPP scheme on a quasi-global oceanic general circulation model are examined by carrying out four test cases. To evaluate simulated upper layer temperature and surface mixed-layer depth (MLD), the model seasonal cycle of temperature and MLD are compared with those from Levitus climatology. In this study, the MLD is defined as the depth that the temperature has changed 0.8°C from the reference depth of 10 m. Statistic analysis shows that test cases with the addition of wave-induced vertical mixing can reduce the root-mean-square difference of upper layer temperature and increase the correlation with Levitus climatology. On the basis of the comparison with Levitus climatology, the surface-wave-induced mixing improves the simulation of MLD in summertime for both hemispheres. Comparing the MLD in different seasons, the wave-induced mixing improves MLD in both hemispheres in summer more than in other seasons. The simulation results are sensitive to weighting coefficients of the wave-induced mixing, suggesting that a preferred weighting coefficient be between 0.1 and 0.3 in the modified KPP scheme.

Citation: Wang, Y., F. Qiao, G. Fang, and Z. Wei (2010), Application of wave-induced vertical mixing to the K profile parameterization scheme, *J. Geophys. Res.*, *115*, C09014, doi:10.1029/2009JC005856.

1. Introduction

[2] Many ocean modeling studies in literature have focused on understanding the ocean's role in climate change. From this point of view, sea-surface temperature (SST) and ocean MLD are key variables because they directly reveal the interaction between the ocean and the atmosphere [*Schopf and Loughe*, 1995; *Kara et al.*, 2003]. In order to predict SST and MLD as accurately as possible, it is necessary to study upper ocean mixed-layer physics and parameterize related vertical mixing processes [*McWilliams*, 1996]. A variety of vertical mixing schemes have been developed and tested [e.g., *Pacanowski and Philander*, 1981; *Mellor and Yamada*, 1982; *Fang and Ichiye*, 1983; *Price et al.*, 1986; *Chen et al.*, 1994; *Large et al.*, 1994]. However, the nonbreaking surface-wave-induced vertical mixing was not fully considered on these mixing schemes. It is believed that surface waves can enhance mixing in the upper ocean, and the wave-induced mixing can improve the simulation of seasonal variations for upper layer temperature and MLD [*Qiao et al.*, 2004a]. The key is how to parameterize mixing processes and combine the parameterization with existing mixing schemes. By considering the surface-wave-induced fluctuation u_{iw} in the Reynolds stress analysis, *Qiao et al.* [2004a, 2008] obtained the expression of nonbreaking wave-induced mixing (*Bv*; following the abbreviated form of *Qiao et al.* [2004a]) and applied *Bv* to an ocean general circulation model (OGCM) with the Mellor-Yamada mixing scheme. Their model results showed much improved simulations of MLD and SST. This kind of wave-induced turbulence unrelated to wave breaking was observed in ingeniously designed laboratory experiments [*Babanin and Haus*, 2009; *Dai et al.*, 2010]. Numerical experiments have shown that wave-induced vertical mixing plays a key role in the climate system [*Song et al.*, 2007; *Babanin et al.*, 2009].

[3] As one of the popular vertical mixing schemes, the K profile parameterization (KPP) scheme [*Large et al.*, 1994] has gained respect as an alternative in deep ocean applications [*Large and Gent*, 1999; *Durski et al.*, 2004]. In the KPP scheme, turbulence of the oceanic surface boundary layer (OBL) is driven primarily by the surface stress τ_0 and surface buoyancy flux B_f; for the ocean interior, the mixing due to shear instability, internal wave breaking, and double diffusion are considered. The OBL turbulence parameterization of KPP is derived from the *Troen and Mahrt* [1986] atmospheric boundary layer model with some additional desirable features [see *Large et al.*, 1994]. Since the wave-induced mixing is not explicitly considered by the KPP scheme, this study will assess the applicability of adding wave-induced mixing to the KPP scheme.

[4] This paper is organized as follows. Section 2 introduces the model configuration and parameters. Section 3

[1]Key Laboratory of Marine Science and Numerical Modeling, First Institute of Oceanography, State Oceanic Administration, Qingdao, China.

0148-0227/10/2009JC005856

Table 1. Weighting Coefficient of Wave-Induced Mixing for the Control Run and Sensitive Runs[a]

Run Cases	CR	SR[1]	SR[3]	SR[f]
Weighting coefficient α	-	0.1	0.3	1

[a]CR stands for control run and SR stand for sensitive run.

presents comparisons of simulated SST and MLD with climatological SST and MLD. The conclusions of this study are given in section 4.

2. Model Configuration and Parameters

[5] The Regional Oceanic Modeling System (ROMS) is used in this study. ROMS is a community model shared by a large user group around the world, with applications ranging from studying an entire ocean basin to a coastal subregion [*Haidvogel et al.*, 2000; *Penven et al.*, 2001; *Marchesiello et al.*, 2003]. It solves incompressible, hydrostatic, primitive equations with free sea surface, horizontal curvilinear coordinates, and a generalized terrain-following vertical coordinate that can be configured to enhance resolutions near sea surface or seafloor. The model domain used for this study includes the quasi-global ocean from 78°S to 65°N with a horizontal resolution of $^1/_2 \times {}^1/_2°$. Twenty terrain-following s-coordinate levels provide high resolution near the surface. The stretching parameter for the vertical grid [*Song and Haidvogel*, 1994] are $\theta_s = 7$ and $\theta_b = 0.2$. Bathymetry data is derived from the ETOPO5 data set. The model is forced with surface wind stress, heat and freshwater fluxes, and heat flux sensitivity to SST from the Comprehensive Ocean-Atmosphere Data Set ocean surface monthly climatology [*Da Silva et al.*, 1994]. Cyclic boundary condition is used for the east-west boundaries, and the closed boundary conditions are used for the north and south boundaries. Initial conditions are obtained from Levitus climatology [*Levitus and Boyer*, 1994].

[6] The KPP mixing scheme is applied in the model with the common setting. The KPP scheme separates parameterizations of vertical mixing into two distinct parts: one for the ocean interior and the other for the OBL above the boundary layer depth. The formulations of vertical viscosity and diffusivities above h_{sbl} can be expressed as the product of turbulent velocity scales w_M and w_τ and a nondimensional vertical shape function $G(\sigma)$. The vertical mixing below the OBL is given by adding the effects of the local Richardson number instability due to resolved vertical shear, internal wave breaking, and double diffusion.

[7] In addition, the wave-induced mixing Bv is also included, which is simply added to the KPP-derived vertical viscosity and diffusivity. Bv is developed by *Qiao et al.* [2004a] as the following equation:

$$B_v = \alpha \iint_{\vec{k}} E\left(\vec{k}\right) \exp(2kz) d\vec{k} \frac{\partial}{\partial z} \cdot \left[\iint_{\vec{k}} \omega^2 E\left(\vec{k}\right) \exp(2kz) d\vec{k} \right]^{1/2}, \quad (1)$$

where $E(\vec{k})$ represents wave number spectrum, ω is the wave angular frequency, k is the wave number, α is a constant coefficient, and z is the vertical coordinate axis (downward positive) with $z = 0$ at the surface. Bv is expressed as the function of the wave number spectrum, and it can be computed directly by the Key Laboratory of Marine Science and Numerical Modeling (MASNUM) wave number spectrum model [*Yuan et al.*, 1991; *Yang et al.*, 2005], because this model is formulated in terms of wave number spectrum. In fact, Bv can also be computed by other wave models, such as the Wave Model (WAM) [*Wamdi Group*, 1988]. But the frequency directional spectrum should be converted to the wave number spectrum first as,

$$E(\vec{K})d\vec{K} = F(f,\theta)dfd\theta, \quad (2)$$

then Bv can be integrated by equation (1). The temporal and spatial distributions of Bv used in this study are same as those used by *Qiao et al.* [2004a].

[8] To discuss the effect of Bv and evaluate its application, several cases are designed in this study. The first case is the control run with the original KPP scheme; others are sensitive runs with the modified KPP scheme. The sensitive runs are designed by the following considerations:

[9] 1. Since the wave-induced mixing is not explicitly considered in the KPP scheme, has the wave-induced mixing process been merged into the KPP scheme implicitly?

[10] 2. In equation (1), α is an unknown constant coefficient; what value of α is conformable to the KPP scheme?

[11] In this study, the sensitive runs are designed with a different setting of α. The α can be regarded as weighting coefficients of the wave-induced mixing.

[12] Since *Qiao et al.* [2004a] set $\alpha = 1$ to the Mellor-Yamada scheme and got an improvement for the simulation of temperature in the upper 100 m, we set the same value of α as one of sensitive runs. The model results show some overestimate vertical mixing area by comparing with the Levitus climatology [*Levitus and Boyer*, 1994]. After that, we ran a series of sensitive runs with a different setting of α and selected three typical cases to discuss the application of wave-induced vertical mixing to the KPP scheme in this study. Each value of α for the sensitive runs is listed in Table 1. In this paper, we use CR to indicate a control run and SRs to indicate sensitive runs. All cases have been run for 15 years each, and the results in the 15th year are used for analysis.

[13] Figure 1a shows the distribution of h_{sbl} in August derived from a CR. It can be seen that h_{sbl} is less than 10 m for the main part of the Northern Hemisphere in boreal summer. In austral summer, h_{sbl} is less than 10 m in nearly all the Southern Hemisphere. It is indicated that the notable vertical mixing was trapped within the near-surface region in the summertime for both hemispheres in the original KPP scheme. Figure 1b is the depth at which K_τ is decreased to 5 $cm^2\ s^{-1}$ (same as the definition of D_5 by *Qiao et al.* [2004a]). The blank area in Figure 1b indicates the vertical diffusivity is less than 5 $cm^2\ s^{-1}$ at the whole water depth. The distributions of h_{sbl} and the depth of $K_\tau = 5\ cm^2/s$ show obvious consistency. Comparing with the global distribution of D_5 in August [*Qiao et al.*, 2004a, Figure 2a], K_τ

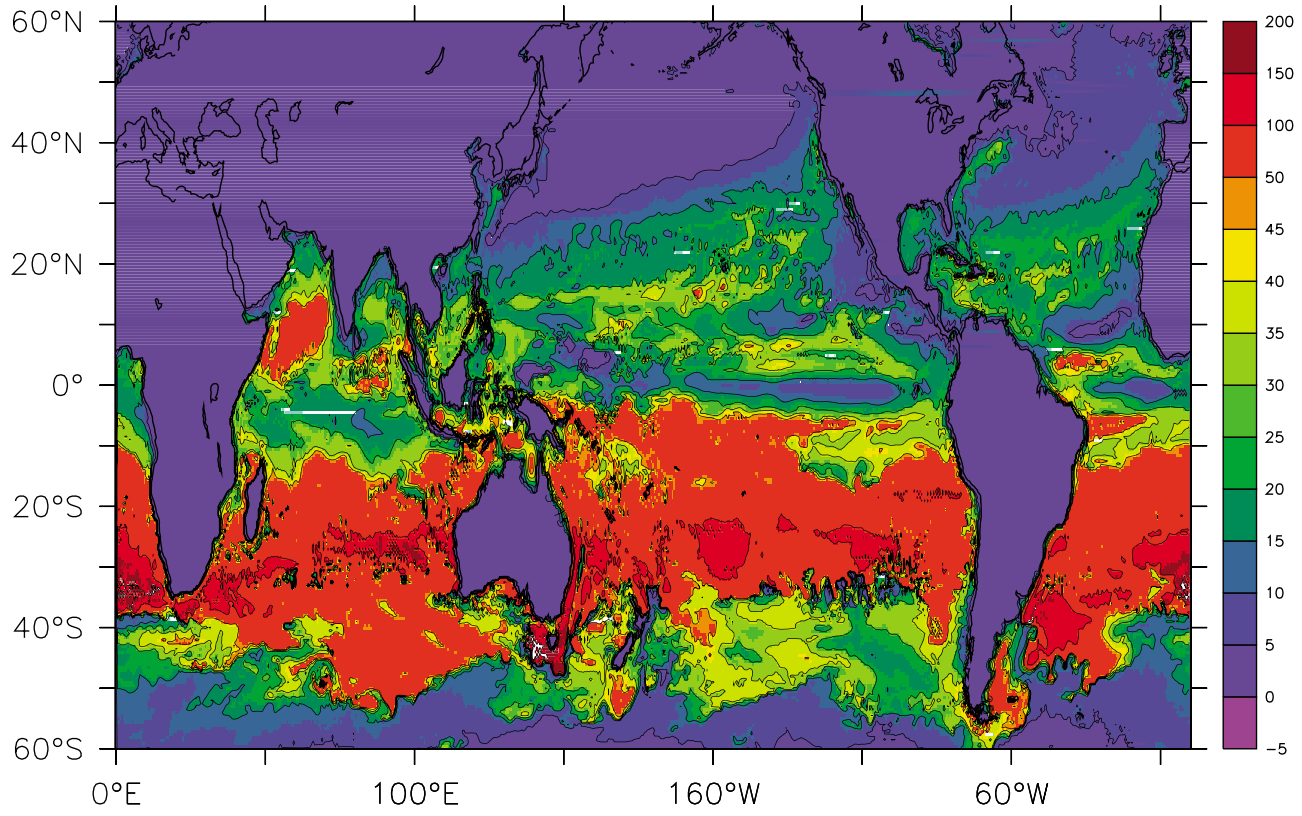

Figure 1a. The distribution of h_{sbl} in August derived from control run.

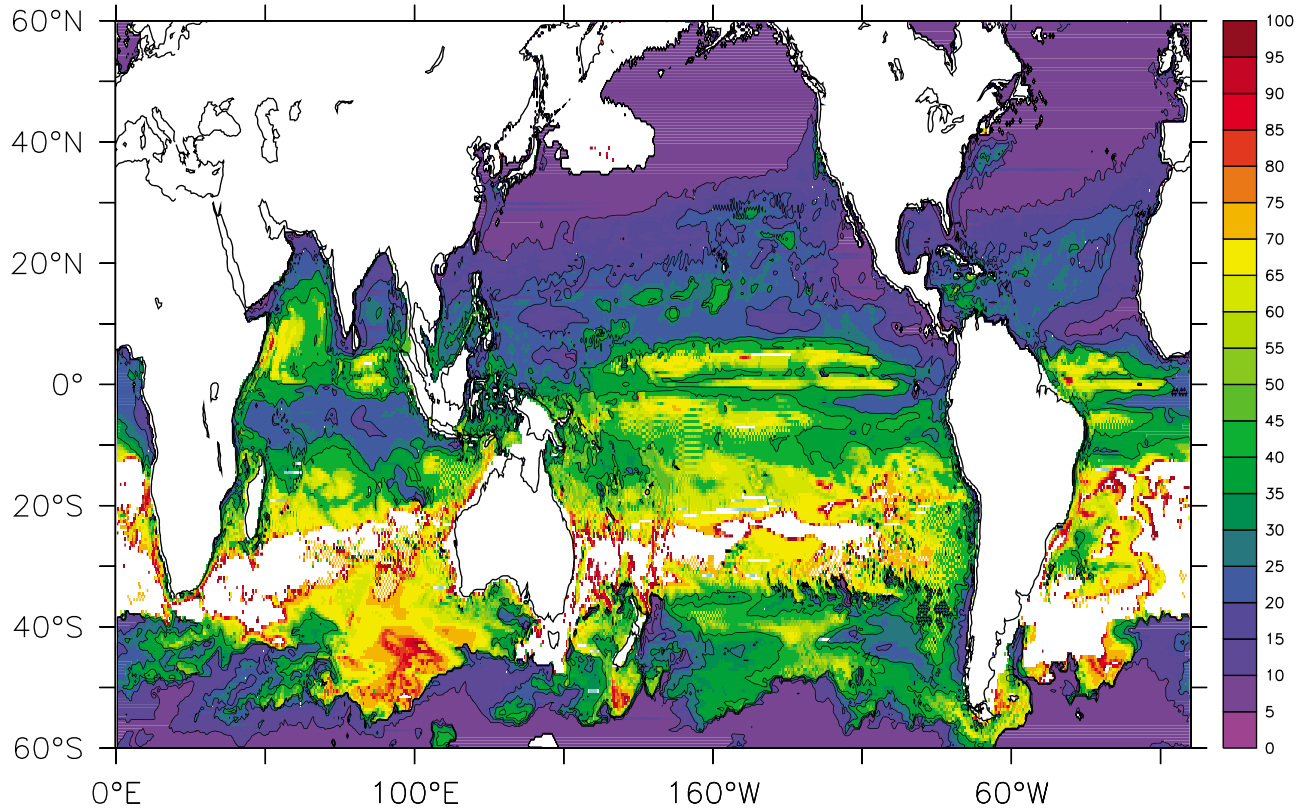

Figure 1b. The depth of $K_\tau = 5$ cm^2/s. The blank area indicates the vertical diffusivity less than 5 cm^2 s^{-1} at the whole water depth.

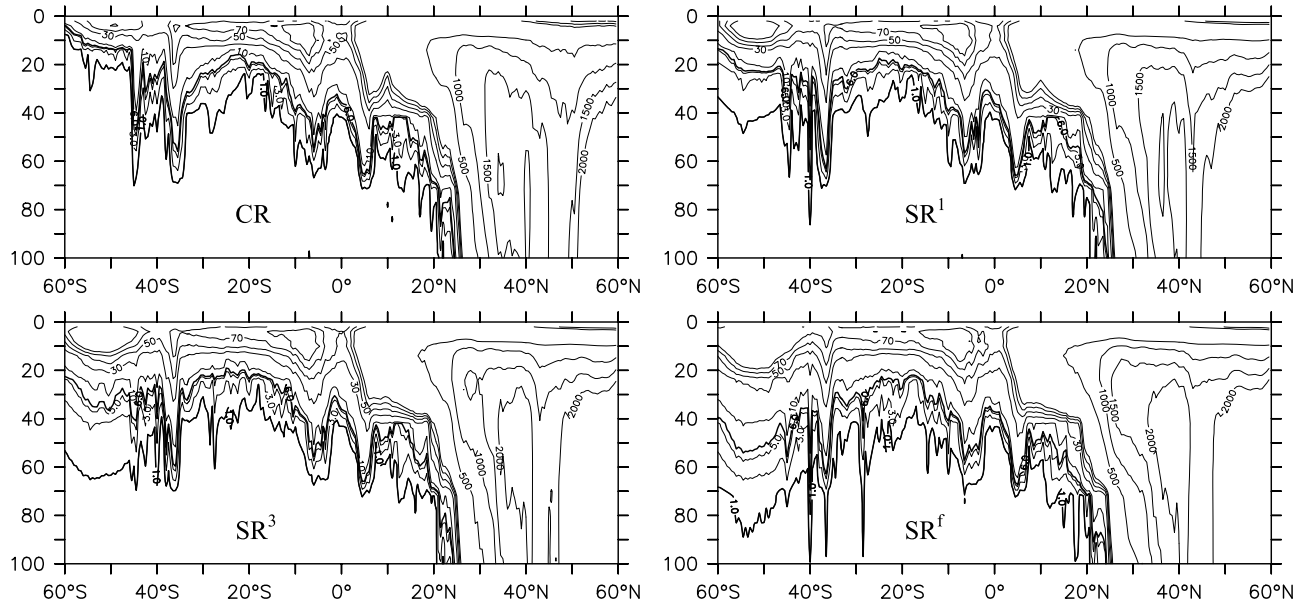

Figure 2a. Zonally averaged distribution of vertical diffusivity K_τ for the control run (CR) and sensitive runs (SRs) in February. Contour interval is 2 cm^2 s^{-1} from 1 to 5 cm^2 s^{-1}, 5 cm^2 s^{-1} from 5 to 10 cm^2 s^{-1}, 20 cm^2 s^{-1} from 10 to 100 cm^2 s^{-1}, and 500 cm^2 s^{-1} from 500 to 2000 cm^2 s^{-1}.

derived from original KPP is less significant than *Bv* in the summertime. Since laboratory experiments by *Dai et al.* [2010] revealed the existence of turbulence induced by nonbreaking surface waves, the original KPP shows some underestimate upper layer vertical diffusivity in the summertime. The vertical diffusivity K_τ in the CR and SRs is shown in Figures 2a and 2b. For convenience, the global ocean is separated into three regions, which are defined as region 1 (RegS; from 60°S to 20°S), region 2 (RegN; from 20°N to 60°N), and region 3 (tropical area from 20°S to 20°N). It can be seen that there is no obvious change between the CR and SRs in region 3 because *Bv* is not comparable with the KPP mixing in the tropics [*Qiao et al.*, 2004a]. For RegS and RegN, however, K_τ displays obvious changes between the CR and SRs, especially for cases with high values of α. For boreal and austral winters, the K_τ in the CR is big enough, and the K_τ in the SRs does not change its spatial distribution. However, for boreal and austral summers, the effect of *Bv* is comparable with the original KPP mixing, and the upper layer distribution of K_τ shows distinct change. To demonstrate the effect of *Bv*, a reference depth is defined, where K_τ = 1 cm^2 s^{-1}. Table 2 shows the

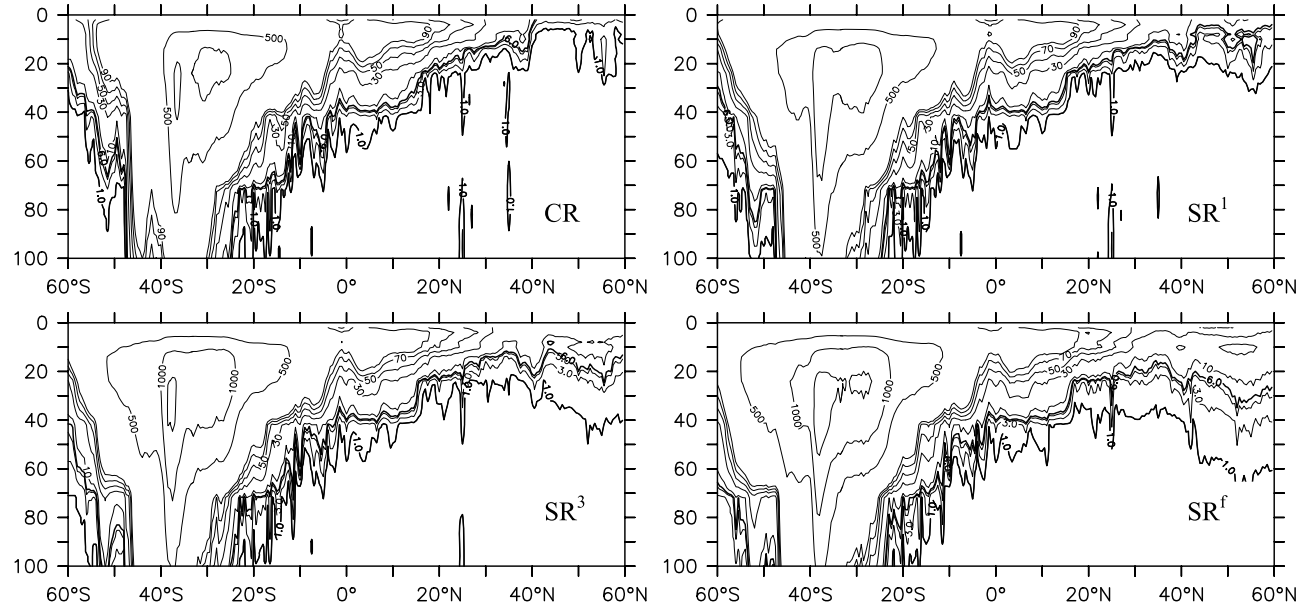

Figure 2b. Same as Figure 2a except for August.

Table 2. Reference Depth in RegS and RegN for the Control Run and Sensitive Runs[a]

Run Cases	CR	SR^1	SR^3	SR^f
RegS in February	15.2	18.4	26.0	37.0
RegN in August	23.3	29.8	36.1	44.3

[a]Depth is give in m. RegS and RegN are from 60 to 20°S and from 20 to 60°N, respectively. CR stands for control run and SR stand for sensitive run. The reference depth is defined as the depth of $K_\tau = 1$ cm^2 s^{-1}.

reference depth from the CR and SRs. It is obvious that the reference depth becomes distinctly bigger with increasing α. A deeper reference depth indicates a stronger mixing process occurring in the upper layer of the ocean.

3. Model-Data Comparison

3.1. Comparison Method

[14] To evaluate the applicability of *Bv*, several statistical methods are used to compare the model outputs and the Levitus climatology. The monthly means of temperature and MLD are considered in this study.

[15] Following the statistical methods of *Kara et al.* [2003], $X_i (i = 1, 2, \ldots, n)$ is a set of reference values (i.e., Levitus temperature), and $Y_i (i = 1, 2, \ldots, n)$ is a set of estimates (i.e., simulated temperature by the CR and SRs). $\overline{X}(\overline{Y})$ and $\sigma_X(\sigma_Y)$ are the mean and standard deviations of the reference (estimates) values, respectively. We evaluate time series of modeled monthly mean temperature from January to December at each grid point over the model domain. Thus, n is 12 in this study. Following the work of *Murphy* [1988] and *Stewart* [1990], the statistical relationship between the Levitus temperature X and the simulated temperature Y can be expressed as follows:

$$ME_i = Y_i - X_i \tag{3}$$

$$\mathrm{RMS} = \left[\frac{1}{n}\sum_{i=1}^{n}(Y_i - X_i)^2\right]^{1/2} \tag{4}$$

$$R = \frac{1}{n}\sum_{i=1}^{n}\frac{(X_i - \overline{X})(Y_i - \overline{Y})}{(\sigma_X \sigma_Y)} \tag{5}$$

$$\mathrm{SS} = R^2 - [R - (\sigma_Y \sigma_X)]^2 - [(\overline{Y} - \overline{X})/\sigma_X]^2 \tag{6}$$

where ME_i is the bias of the ith month, RMS is the root-mean-square difference, R is the correlation coefficient, and SS is the skill score. For 12 monthly mean temperatures at each grid point over the global ocean, the R value must be at least ±0.53 for it to be statistically different from R = 0 based on the t-test at the 95% confidence level [*Neter et al.*, 1988].

[16] The SS in equation (6) is computed by accounting for two biases termed conditional and unconditional biases [*Kara et al.*, 2003]. Unconditional bias (also called sys-

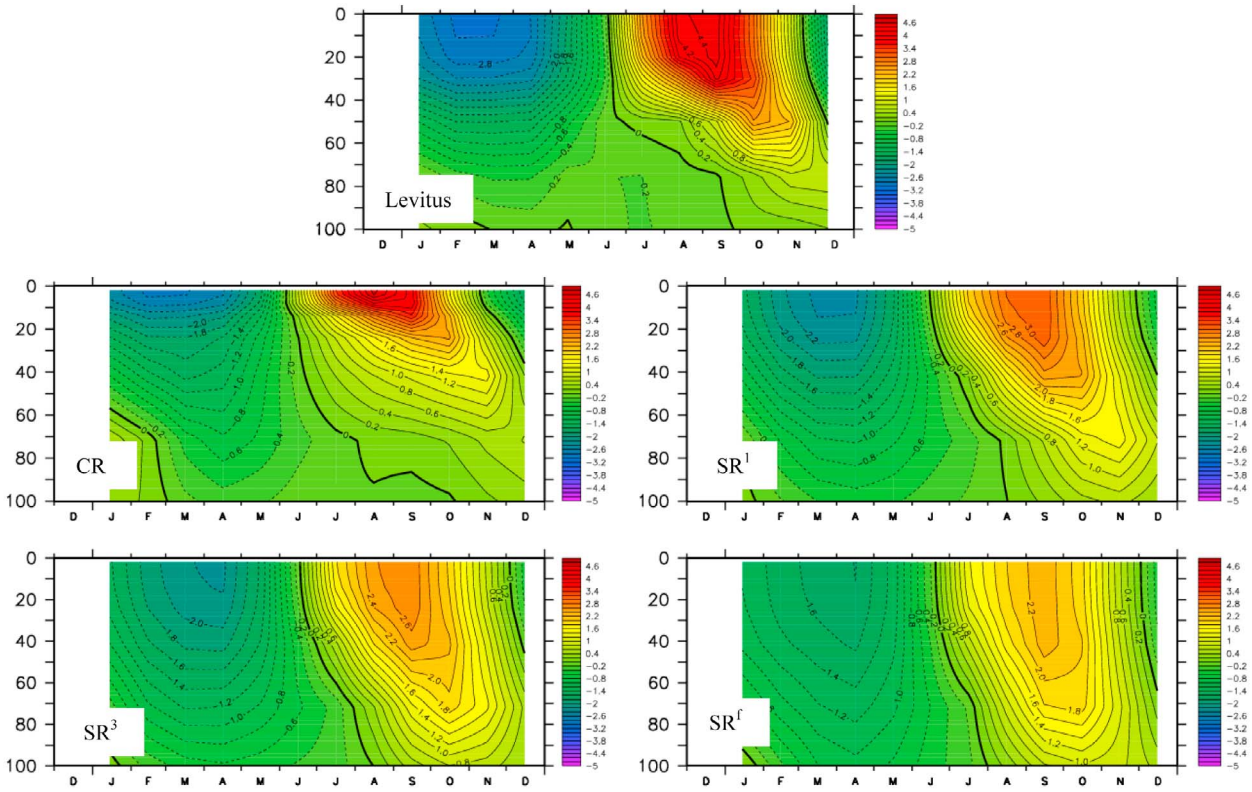

Figure 3a. Comparison of the seasonal variation for upper layer temperature anomalies at 50°N, 145°W (control run, CR; sensitive run, SR).

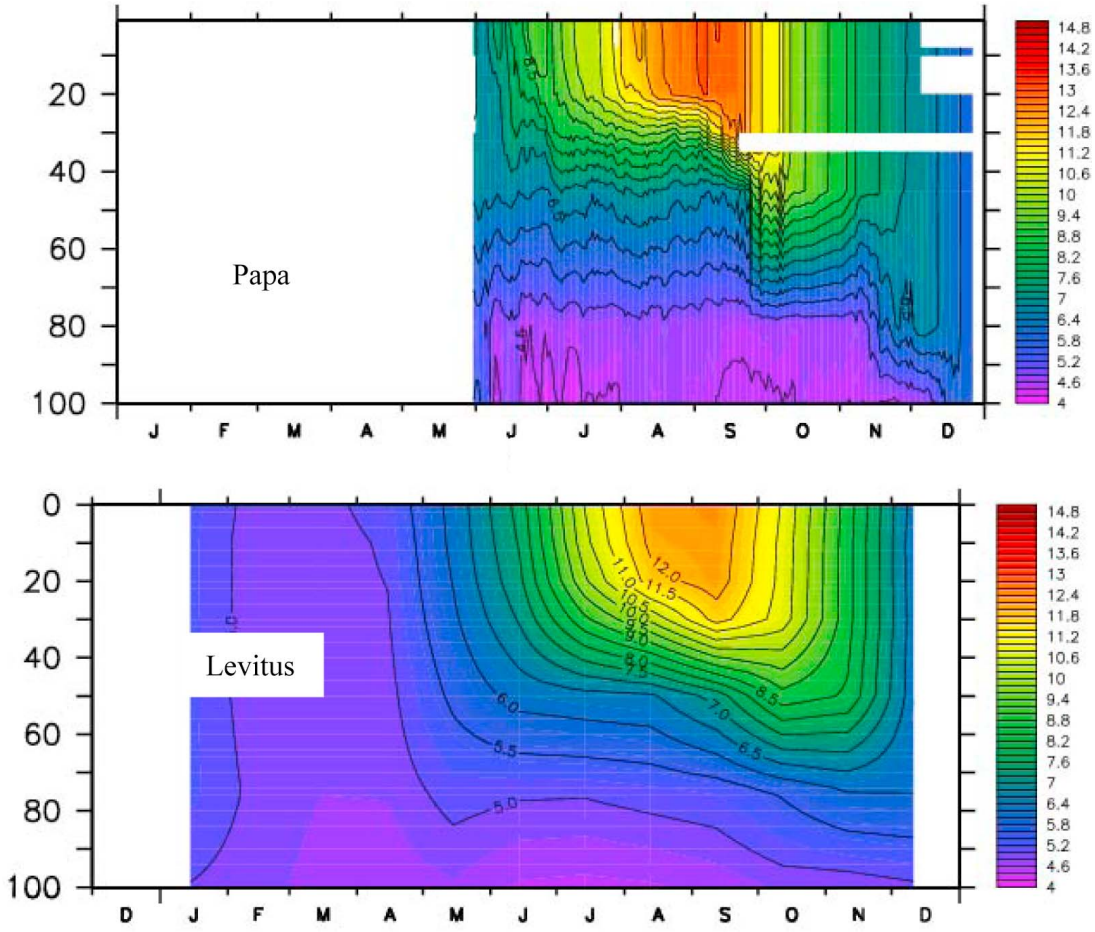

Figure 3b. Comparison of the seasonal variation of upper layer temperature between Levitus data and Ocean Station Papa data.

tematic bias, B_{UC}) is a measure of the difference between the means of simulated temperature, while the conditional bias (B_C) is a measure of the relative amplitude of the variability in the two data sets [*Murphy*, 1992]. The SS based on the RMS difference can be defined as $SS = 1 - RMS^2/\sigma_X^2$, and this is mathematically equivalent to equation (6). The SS is 1.0 for the perfectly simulated temperature [e.g., *Murphy and Daan*, 1985], and positive skill is usually considered to represent a minimal level of acceptable performance. Note that the correlation coefficient squared is equal to SS only when both conditional and unconditional biases are zero. Because the two biases are never negative, the correlation can be considered as a measure of "potential" skill, that is, a skill that can be obtained by eliminating biases from the model. Using the preceding statistical measures, we will next perform model-data comparisons for temperature.

3.2. Comparison for Upper Layer Temperature

[17] Comparison of the seasonal variation for upper layer temperature anomalies at 50°N, 145°W was shown in Figure 3a. For the CR, the isotherm was trapped within the upper 20 m layer. The seasonal variation of SR[1] shows a reasonable fit with the Levitus data. To validate the Levitus data, the seasonal variation of the upper layer temperature observed at Ocean Station Papa is shown in Figure 3b. These two data show essential agreement, except the Levitus data are smoother.

[18] To avoid any contamination of other processes from surface boundary conditions, the 10 m depth temperature of the CR and SRs are compared with the Levitus climatology. February and August are selected as representatives, because these two months are the summertime for each hemisphere, when a large proportion of upper layer vertical mixing is contributed by *Bv*. Figures 4a and 4b shows the comparison of ME_2 and ME_8 (the subscript i represents the ith month) for the CR and SRs at a 10 m depth. In RegS, the ME_2 of the CR shows much discrepancy south of 45°S. However, the ME_2 of the SRs seems better. This improvement is mainly due to incorporating *Bv* to the vertical mixing scheme. At the austral summertime, the surface layer is stable stratification with low salinity and high temperature in RegS, accompanying a small h_{sbl} (less than 10 m) in the original KPP scheme. The depth of $K_\tau = 1$ cm^2 s^{-1} is about 20 m in CR (Figure 2a) south of 45°S. The warm water was trapped at the upper 40 m and, therefore, an overestimated temperature exists south of 45°S at 10 m depth in CR. After

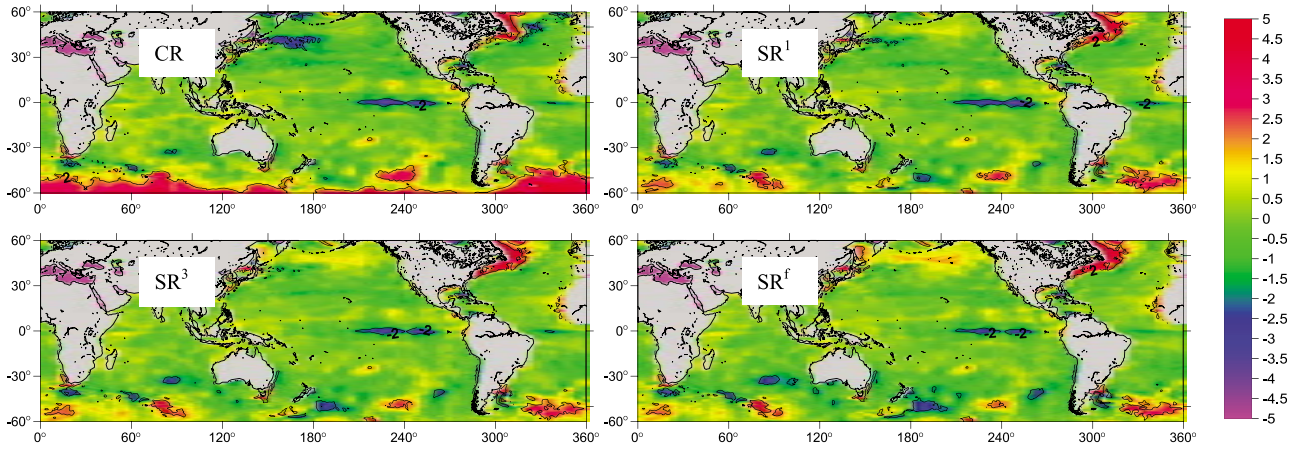

Figure 4a. The mean bias in February between model and Levitus climatology at 10 m. Positive values for model are warmer than Levitus (control run, CR; sensitive run, SR).

incorporating Bv to the vertical mixing scheme, the K_τ is big enough to mix the upper water with the lower water and improve the thermal structure for the Southern Ocean. In RegN, ME_2 shows much discrepancy in the northwest Atlantic. It is mainly due to the close boundary condition at 65°N. In the northeast Pacific, an overestimated area appears gradually with the increasing of the effect of Bv (i.e., increasing the value of α). The vertical profile of the regional average (180°E–130°W, 40–60°N, see Figure 5) temperature for the northeast Pacific shows a maximum temperature existed at the depth of about 100 m. As the ocean loses heat in the northern Pacific in February, the stronger vertical mixing can compensate the losing heat from lower water and leads to a higher temperature in the upper layers.

[19] The upper layer temperature differences in August are shown in Figure 4b. In RegS, there are not any differences between the CR and SRs. In RegN, a large underestimated area exists north of 30°N in the northwest Pacific. This underestimated area was reduced in the SR with α = 0.1, but it increases again with the increasing of the value of α. In boreal summer, the h_{sbl} is quite shallow (less than 5 m, see Figure 1a) in RegN, corresponding with a weak vertical mixing in CR, especially between 40–50°N (Figure 2b) where it fits with the underestimated area in CR. The depth of K_τ = 1 cm^2 s^{-1} is less than 10 m in CR; therefore, an underestimated temperature exists at 10 m. After incorporating Bv to the vertical mixing scheme with α = 0.1, the upper mixed layer becomes deeper than the CR (about 20–30 m), and the underestimated area was reduced. With the increasing of the value of α, the upper mixed layer becomes so deep that the upper layer temperature was underestimated by the excess heat transmitting from the upper layer to lower layer.

[20] Figure 6 exhibits the RMS for the CR and SRs. The same as the upper layer temperature, the significantly improved areas are the Southern Ocean and the northwest Pacific. Table 3 lists the regional average RMS for the CR

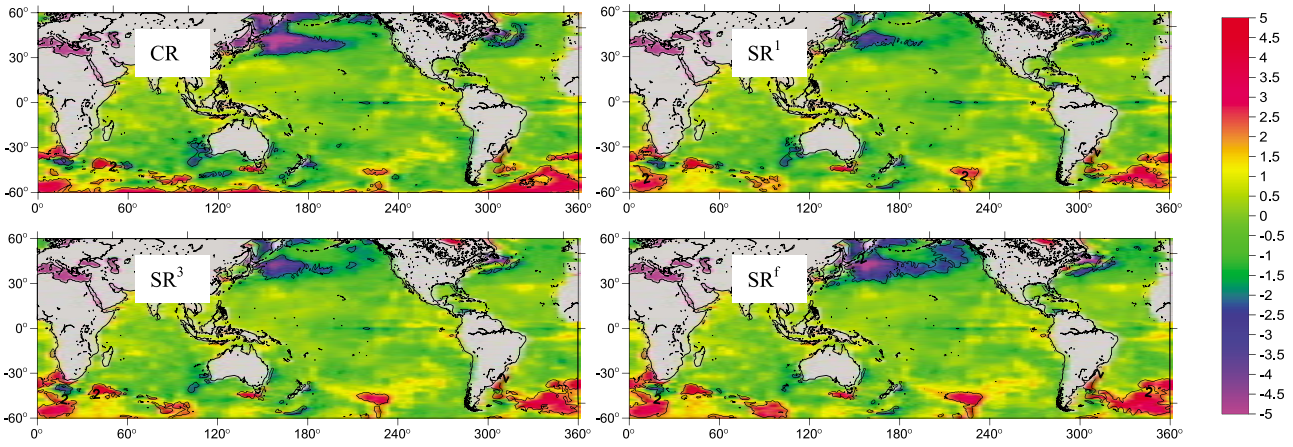

Figure 4b. Same as Figure 4a except for August.

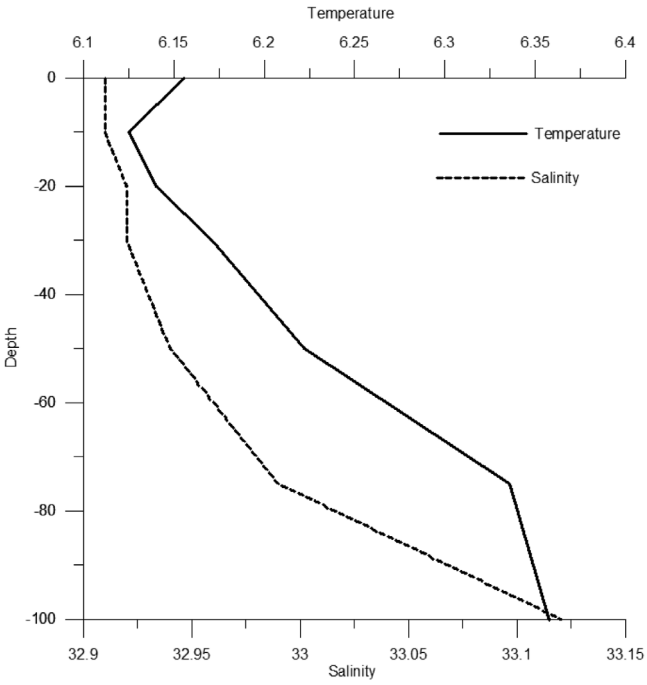

Figure 5. Comparison of root-mean-square between the control run and the sensitive runs at 10 m depth.

and SRs. It can be seen that the SR with $\alpha = 0.1$ is the most favorable one; it reduces the RMS of RegS from 1.09 to 0.89°C and the RMS of RegN from 1.0 to 0.85°C.

[21] After comparing with the upper layer temperature (at 10 m depth), the average correlation coefficients (equation (5)) for RegS and RegN are calculated for the upper 100 m depth, which shows the critical level for the confidence level of 95% by *t* test (Figure 7). Each correlation coefficient of the SRs is remarkably higher than the correlation coefficient of the CR in the full upper 100 m depth, which exhibits that *Bv* can improve the simulated temperature structure for the entire upper layer. According to comparisons of the upper layer temperature with the

Table 3. Regional Average of Root-Mean-Square for the Control Run and Sensitive Runs at 10 m, the Regional and Vertical Average of Correlation Coefficient for the CR and SRs[a]

	Region	CR	SR^1	SR^3	SR^f
RMS	RegS	1.09	0.89	0.92	0.97
	RegN	1.00	0.85	0.91	1.04
Correlation coefficient	RegS	0.68	0.80	0.83	0.83
	RegN	0.82	0.90	0.91	0.89

[a]RMS stands for root-mean-square, CR stands for control run, and SR stands for sensitive run. Vertical average is for top 100 m. RegS and RegN are from 60 to 20°S and from 20 to 60°N, respectively.

Levitus data, the higher correlation coefficient of SRs is mainly due to the improvement of the vertical structure of the summertime temperature. In RegS (Figure 7a), the correlation coefficient of the CR reaches the critical level at about 70 m. That means, under this depth, the simulated seasonal variation of the temperature is not significantly correlated with the Levitus data. However, after considering the effect of *Bv*, the critical depth can reach about 100 m. Thinking over the difference value of α for *Bv*, there are some differences between them: the higher the value of α, the more significant the correlation is for the depth greater than 50 m. In RegN (Figure 7b), all of the correlation coefficients of the SRs are higher than the correlation coefficient of the CR at the full upper 100 m depth as well. Unlike with RegS, there is no obvious difference between SRs. The top 100 m average of the correlation coefficient for the CR and SRs are listed in Table 3. It can be seen that SRs improve the correlation coefficient of RegS from 0.68 to greater than 0.8 and for RegN from 0.82 to ~0.9.

[22] The regional averages of the statistical measures mentioned in section 3.1 (SS, B_C, and B_{UC}) are calculated for RegS and RegN and shown in Figure 8. In RegS, the SS of the SRs is more desirable than the SS of the CR, except in the surface area (0–20 m). In Figure 8a, a turning point exists near the 35 m depth. Up to this depth, the lower the value of α, the better the SS and the better the model performance. On the contrary, below this depth, the higher

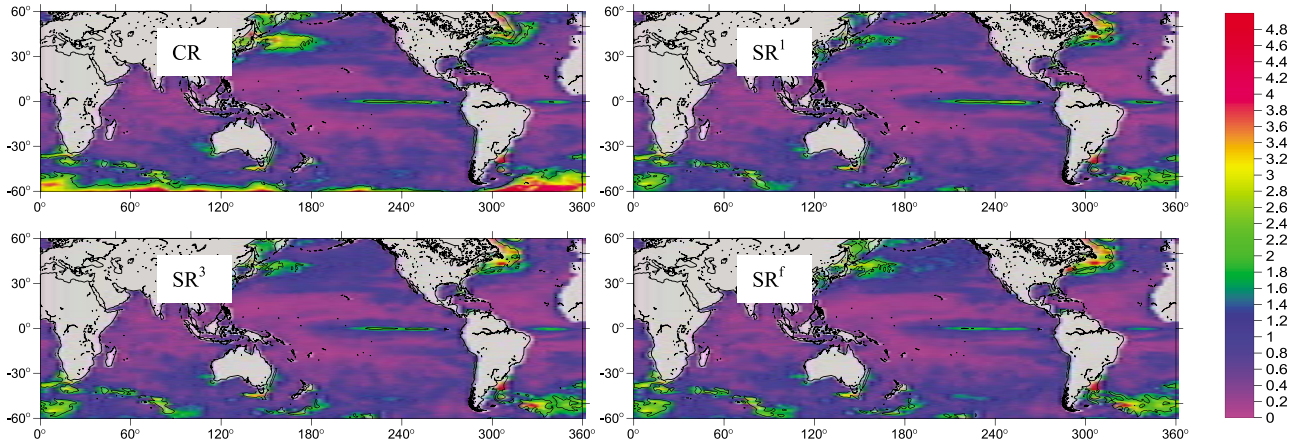

Figure 6. The vertical profile of the regional average (180°E–130°W, 40–60°N) temperature and salinity in February (control run, CR; sensitive run, SR).

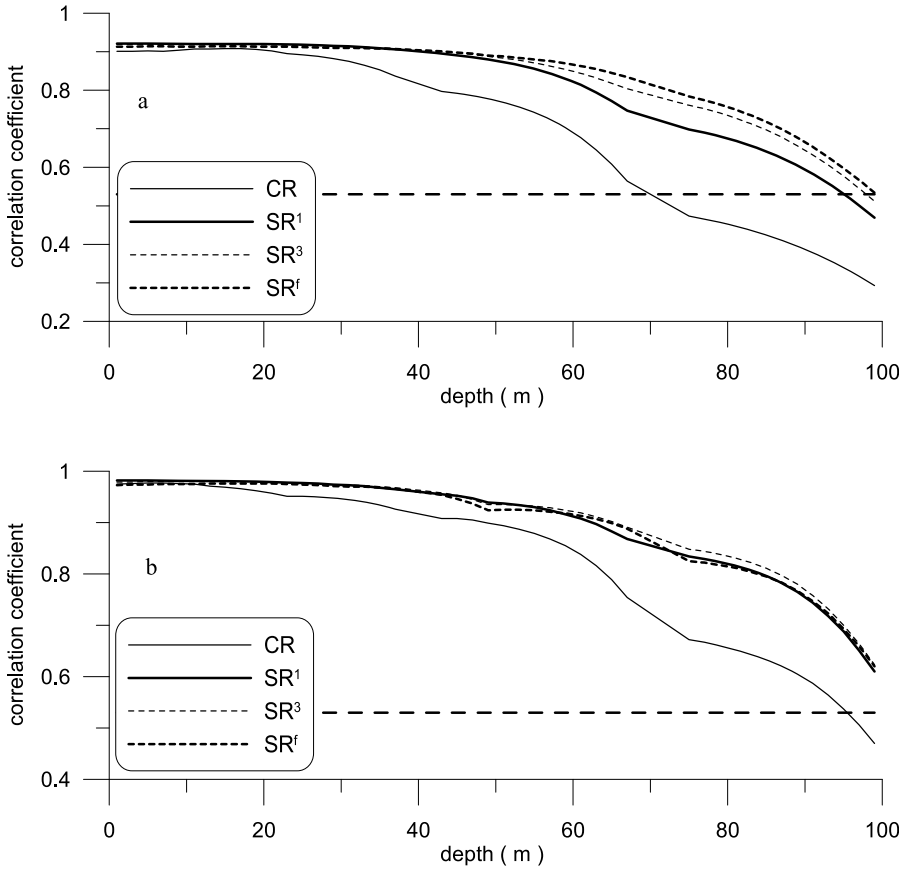

Figure 7. (a) The regional average over RegS (from 60 to 20°S) of correlation coefficient for temperature between the simulated and Levitus versus depth from 0 to 100 m. Values above the dashed line at 0.53 are statistically significant. (b) Same as Figure 7a except for RegN (from 20 to 60°N).

value of α exhibits better skill for simulating the temperature. Figure 8b shows the B_C values in RegS. Since B_C is a measure of the relative amplitude of temperature between the simulated and Levitus data, the decrease of B_C indicates that *Bv* can improve the simulation of temperature for seasonal variation. Figure 8c shows the values of B_{UC} in RegS. The B_{UC} values of the SRs are better than those of the CR below a 15 m depth. Since B_{UC} is a measure of the difference between the means of temperature between the simulated and Levitus data, the change of B_{UC} indicates that *Bv* can improve the simulation of temperature for annual mean values. The SS in RegN shows as more applicable than that in RegS. In Figure 8d, most depths show great improvement for the skill of simulating temperature. Figure 8e shows the B_C values in RegN. The change of B_C indicates that *Bv* can improve the simulation of temperature for seasonal variation. Figure 5f shows the B_{UC} values in RegN. The B_{UC} values of the SRs are better than those of the CR, except in near-surface areas. The change of B_{UC} indicates that *Bv* can improve the simulation of temperature for annual mean values in RegN.

3.3. Comparison for MLD

[23] In this section, monthly mean MLD values obtained from the CR and SRs are compared to those obtained from the Levitus climatology. Owing to the fact that the MLD is very deep in winter time for both hemispheres, only the summertime MLD is shown. In this study, the MLD is defined as the depth that the temperature has changed 0.8°C from the reference depth of 10 m.

[24] Figure 9a shows the distribution of MLD for the Levitus data, the CR and SRs for RegS in February; Figure 6b shows the distribution of MLD for RegN in August. For the summertime in the Southern Hemisphere (Figure 9a), the MLD of the CR is shallower than the Levitus between 20 and 40°S. After incorporating *Bv* to the mixing scheme, the MLD of the SRs with α = 0.1 and 0.3 are more comparable to that of Levitus than the MLD of the CR. However, the SR with α = 1.0 shows some overestimated MLD in the Southern Ocean. For the summertime of the Northern Hemisphere (Figure 9b), the MLD of the CR is shallower than the Levitus north of 25°N. After considering *Bv* in the mixing scheme, both the values and distributions of the MLD of the SR with α = 0.1 are improved significantly. For big values of α, however, an overestimated tendency is obvious.

4. Summary and Conclusions

[25] In this study, the wave-induced mixing is incorporated into the KPP scheme to study its impact on upper ocean processes. One CR and three SRs with different

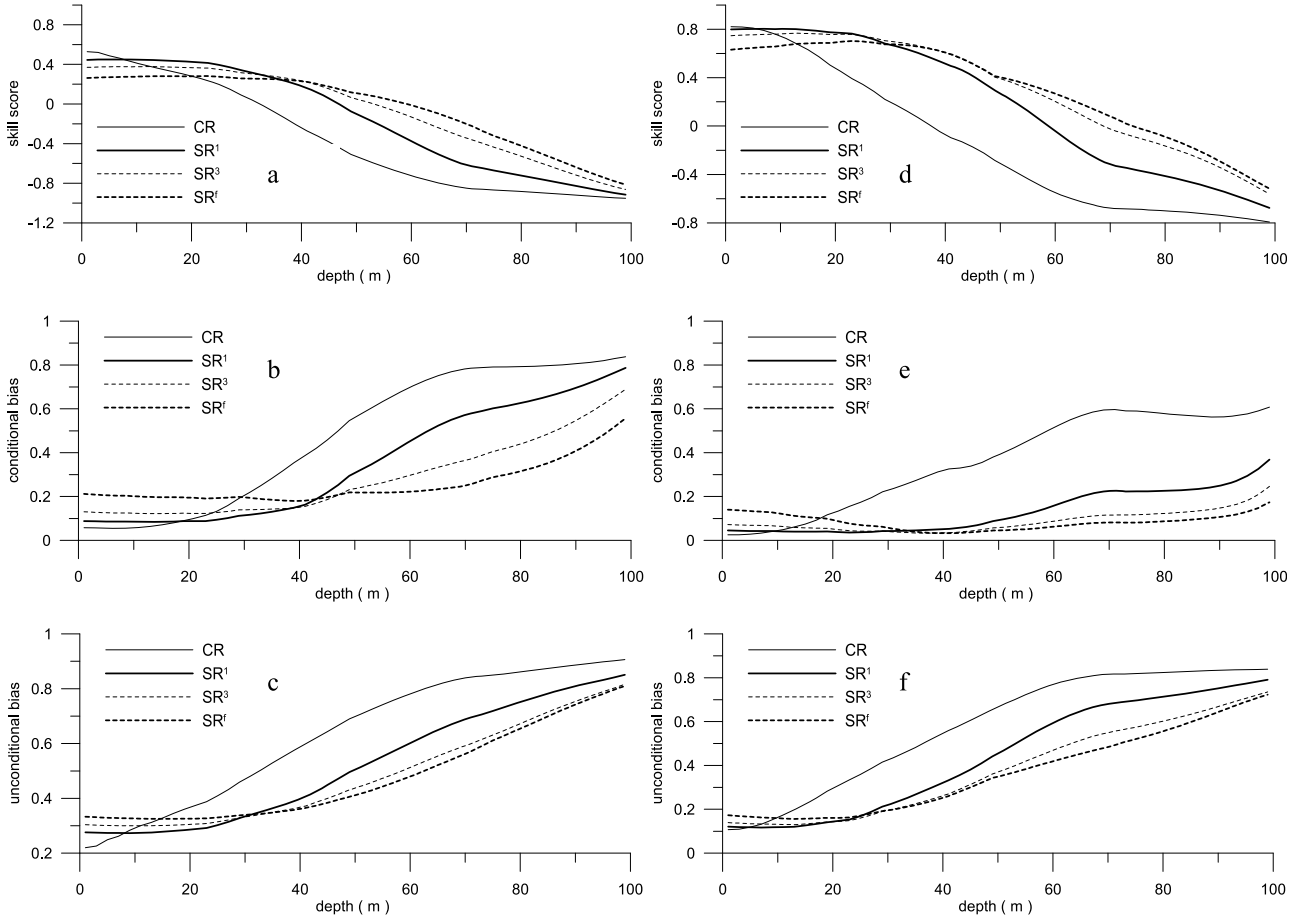

Figure 8. The regional average of skill score, conditional bias, and unconditional bias for temperature between the simulated and Levitus data versus depth from 0 to 100 m (control run, CR; sensitive run, (SR)). The regional average of (a) skill score over RegS (from 60 to 20°S), (b) conditional bias over RegS, (c) unconditional bias over RegS, (d) skill score over RegN (from 20 to 60°N), (e) conditional bias over RegN, and (f) unconditional bias over RegN.

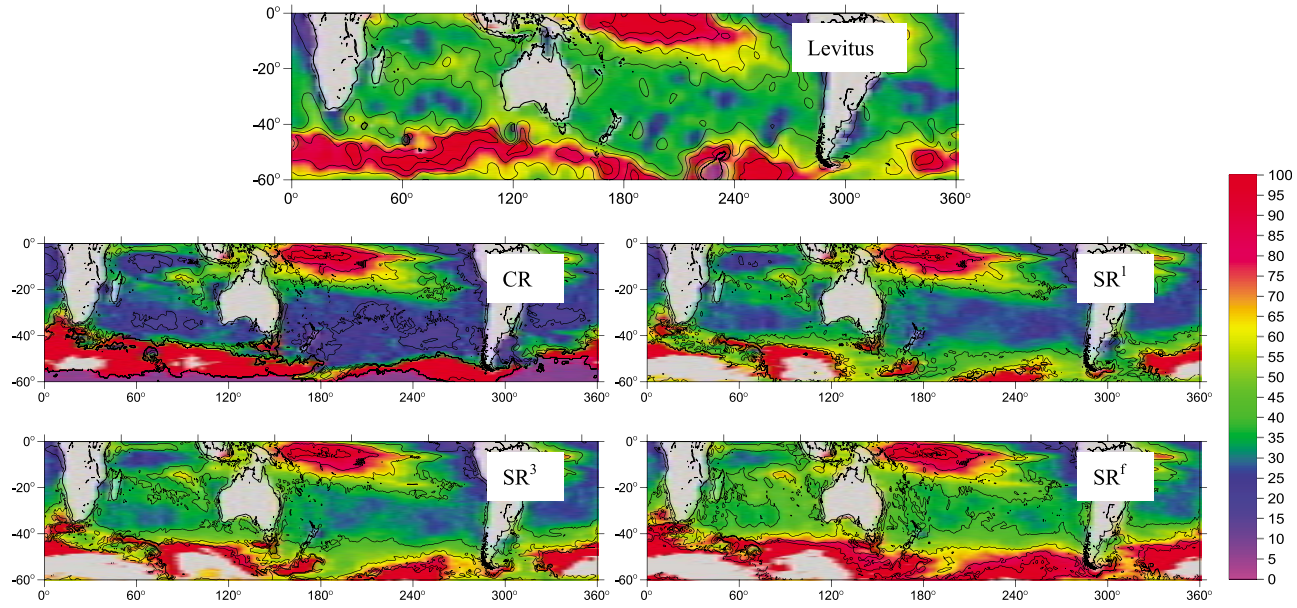

Figure 9a. Distributions of mixed-layer depth (MLD) of RegS (from 60 to 20°S) in February. The MLD is defined as the depth at which the temperature decreased 0.8°C from the reference depth of 10 m (control run, CR; sensitive run, SR).

effects of the wave-induced mixing are carried out. Comparison of the model results shows the following. The modified KPP scheme can improve the simulation of the upper layer temperature and the MLD in midlatitudes and high latitudes for RegS and RegN. Thinking over the effect of the different value of α for the wave-induced mixing, the reasonable value of α should be between 0.1 and 0.3 in the KPP scheme.

[26] This study focuses on the application of the wave-induced mixing in the KPP scheme in an OGCM. In a coastal area or a regional basin, the application of the wave-induced mixing in the KPP scheme needs further study. Some related work has been done on the Mellor-Yamada scheme, giving some reasonable results [*Qiao et al.*, 2004b, 2006; *Xia et al.*, 2006].

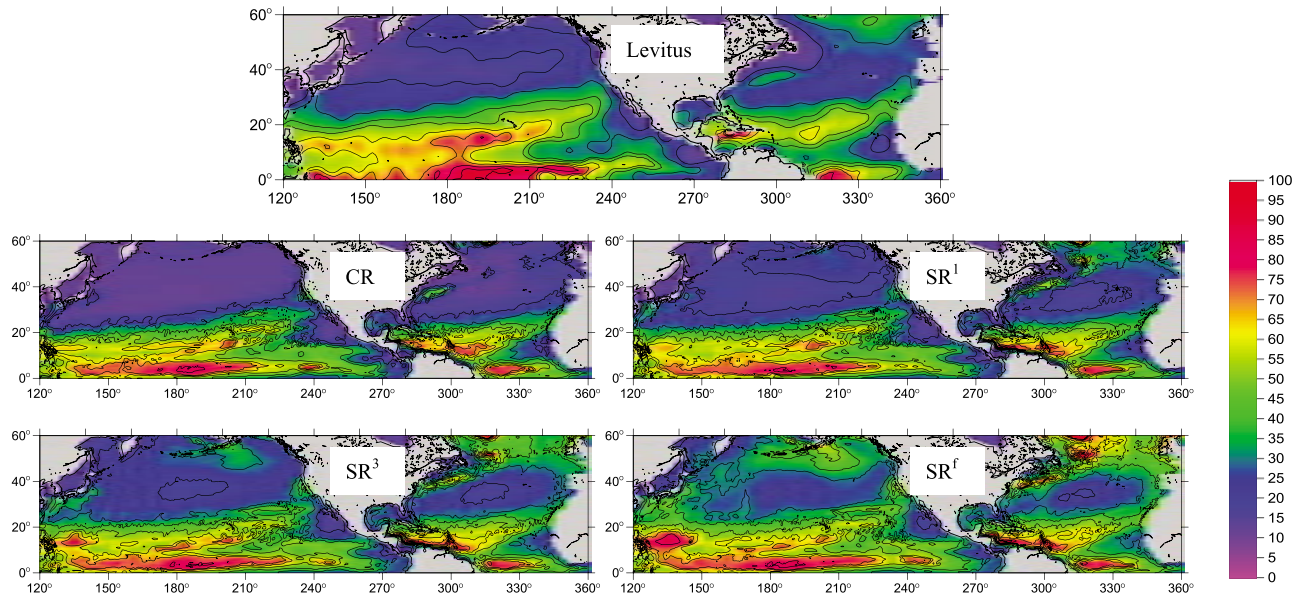

Figure 9b. Same as Figure 9a except for RegN (from 20 to 60°N) in August.

[27] **Acknowledgments.** This research was supported by the National Natural Science Foundation of China through grants 40730842 and 40606006. The authors wish to thank the reviewers for their constructive comments. Thanks to the Papa Project Office for providing in situ data (http://www.pmel.noaa.gov/stnP/data.html).

References

Babanin, A. V., and B. K. Haus (2009), On the existence of water turbulence induced by non-breaking surface waves, *J. Phys. Oceanogr.*, *39*, 2675–2679, doi:10.1175/2009JPO4202.1.

Babanin, A. V., A. Ganopolski, and W. R. C. Phillips (2009), Wave-induced upper-ocean mixing in a climate model of intermediate complexity, *Ocean Modell.*, *29*, 189–197, doi:10.1016/j.ocemod.2009.04.003.

Chen, D., A. J. Busalacchi, and L. M. Rothstein (1994), The roles of vertical mixing, solar radiation, and wind stress in a model simulation of the sea surface temperature seasonal cycle in the tropical Pacific Ocean, *J. Geophys. Res.*, *99*, 20,345–20,359, doi:10.1029/94JC01621.

Dai, D., F. Qiao, W. Sulisz, L. Han, and A. Babanin (2010), An experiment on the non-breaking surface-wave-induced vertical mixing, *J. Phys. Oceanogr.*, doi:10.1175/2010JPO4378.1, in press.

da Silva, A. M., C. C. Young-Molling, and S. Levitus (1994), *Atlas of Surface Marine Data 1994*, vol. 1, *Algorithms and Procedures*, *NOAA Atlas NESDIS*, vol. 6, 83 pp., NOAA, Silver Spring, Md.

Durski, S. M., S. M. Glenn, and D. B. Haidvogel (2004), Vertical mixing schemes in the coastal ocean: Comparison of the level 2.5 Mellor-Yamada scheme with an enhanced version of the K profile parameterization, *J. Geophys. Res.*, *109*, C01015, doi:10.1029/2002JC001702.

Fang, G., and T. Ichiye (1983), On the vertical structure of tidal currents in a homogeneous sea, *Geophys. J. Int.*, *73*, 65–82.

Haidvogel, D. B., H. Arango, K. Hedstrom, A. Beckmann, P. Malanotte-Rizzoli, and S. Shchepetkin (2000), Model evaluation experiments in the North Atlantic Basin: Simulations in non-linear terrain-following coordinates, *Dyn. Atmos. Oceans*, *32*, 239–282.

Kara, A. B, A. J. Wallcraft, and H. E. Hurlburt (2003), Climatological SST and MLD predictions from a global layered ocean model with an embedded mixed layer, *J. Atmos. Oceanic Technol.*, *20*, 1616–1632.

Large, W. G., and P. R. Gent (1999), Validation of vertical mixing in an equatorial ocean model using large eddy simulations with observations, *J. Phys. Oceanogr.*, *29*, 449–464.

Large, W. G., J. C. McWilliams, and S. C. Doney (1994), Oceanic vertical mixing: A review and a model with a nonlocal boundary layer parameterization, *Rev. Geophys.*, *32*, 363–403, doi:10.1029/94RG01872.

Levitus, S., and T. Boyer (1994), *World Ocean Atlas 1994*, vol. 4, *Temperature*, *NOAA Atlas NESDIS*, vol. 4, 129 pp., NOAA, Silver Spring, Md.

Marchesiello, P., J. C. McWilliams, A. Shchepetkin (2003), Equilibrium structure and dynamics of the California Current System, *J. Phys. Oceanogr.*, *33*, 753–783.

McWilliams, J. C. (1996), Modeling the oceanic general circulation, *Annu. Rev. Fluid Mech.*, *28*, 215–248.

Mellor, G. L., and T. Yamada (1982), Development of a turbulence closure model for geophysical fluid problems, *Rev. Geophys.*, *20*, 851–875, doi:10.1029/RG020i004p00851.

Murphy, A. H. (1988), Skill scores based on the mean square error and their relationships to the correlation coefficient, *Mon. Weather Rev.*, *116*, 2417–2424.

Murphy, A. H. (1992), Climatology, persistence, and their linear combination as standards of reference in skill scores, *Weather Forecasting*, *7*, 692–698.

Murphy, A. H., and H. Daan (1985), Forecast evaluation, in *Probability, Statistics, and Decision Making in the Atmospheric Sciences*, edited by A. H. Murphy and R. W. Katz, pp. 379–437, Westview, Boulder, Colo.

Neter, J., W. Wasserman, and G. A. Whitmore (1988), *Applied Statistics*, 1006 pp., Allyn and Bacon, Boston.

Pacanowski, R. G., and S. G. H. Philander (1981), Parameterization of vertical mixing in numerical models of the tropical oceans, *J. Phys. Oceanogr.*, *11*, 1443–1451.

Penven, P., C. Roy, G. B. Brundrit, A. C. de Verdière, P. Fréon, A. S. Johnson, J. R. E. Lutjeharms, and F. A. Shillington (2001), A regional hydrodynamic model of upwelling in the southern Benguela, *S. Afr. J. Sci.*, *97*, 472–475.

Price, J. F., R. F. Weller, and R. Pinkel (1986), Diurnal cycling: Observations and models of the upper ocean response to diurnal heating, cooling and wind mixing, *J. Geophys. Res.*, *91*, 8411–8427, doi:10.1029/JC091iC07p08411.

Qiao, F., Y. Yuan, Y. Yang, Q. Zheng, C. Xia, and J. Ma (2004a), Wave induced mixing in the upper ocean: Distribution and application to a global ocean circulation model, *Geophys. Res. Lett.*, *31*, L11303, doi:10.1029/2004GL019824.

Qiao, F., J. Ma, Y. Yang, and Y. Yuan (2004b), Simulation of the temperature and salinity along 36°N in the Yellow Sea with a wave-current coupled model, *J. Korean Soc. Oceanogr.*, *39*(1), 35–45.

Qiao, F., J. Ma, C. Xia, Y. Yang, and Y. Yuan (2006), Influence of the surface wave-induced and tidal mixing on vertical temperature structure of the Yellow and East China seas in summer, *Prog. Nat. Sci.*, *16*(7), 739–746.

Qiao, F., Y. Yang, C. Xia, and Y. Yuan (2008), The role of surface waves in the ocean mixed layer, *Acta Oceanol. Sin.*, *27*, 30–37.

Schopf, P. S., and A. Loughe (1995), A reduced-gravity isopycnal ocean model: Hindcasts of El Niño. *Mon. Weather Rev.*, *123*, 2839–2863.

Song, Y. T., and D. Haidvogel (1994), A semi-implicit ocean circullation model using a generalized topography following coordinate system, *J. Comput. Phys.*, *115*, 228–248.

Song, Z., F. Qiao, Y. Yang, and Y. Yuan (2007), An improvement of the too cold tongue in the tropical Pacific with the development of an ocean-wave-atmosphere coupled numerical model, *Prog. Nat. Sci.*, *17*(5), 576–583.

Stewart, T. R. (1990), A decomposition of the correlation coefficient and its use in analyzing forecasting skill, *Weather Forecasting*, *5*, 661–666.

Troen, I. B., and L. Mahrt (1986), A simple model for the atmospheric boundary layer: Sensitivity to evaporation, *Boundary Layer Meteorol.*, *37*, 129–148.

Wamdi Group (1988), The WAM model–A third generation ocean wave prediction model, *J. Phys. Oceanogr.*, *18*, 1775–1810, doi:10.1175/1520-0485(1988)018<1775:TWMTGO>2.0.CO;2.

Xia, C., F. Qiao, Y. Yang, J. Ma, and Y. Yuan (2006), Three-dimensional structure of the summertime circulation in the Yellow Sea from a wave-tide-circulation coupled model, *J. Geophys. Res.*, *111*, C11S03, doi:10.1029/2005JC003218.

Yang, Y., F. Qiao, W. Zhao, Y. Teng, and Y. Yuan (2005), MASNUM ocean wave numerical model in spherical coordinates and its application, *Acta Oceanol. Sin.*, *22*, 1–7.

Yuan, Y., Z. Pan, F. Hua, and L. Sun (1991) LAGDF-WAM numerical wave model, *Acta Oceanol. Sin.*, *10*, 483–488.

G. Fang, F. Qiao, Y. Wang, and Z. Wei, Key Laboratory of Marine Science and Numerical Modeling, First Institute of Oceanography, State Oceanic Administration, Hi-Tech Park, 6 Xian-Xia-Ling Rd., Qingdao 266061, China. (qiaofl@fio.org.cn)